The seasonally changing cloud feedbacks contribution to the ENSO seasonal phase-locking

by Dietmar Dommenget and Yanshan Yu

School of Earth, Atmosphere and Environment, Monash University, Clayton, Australia

submitted to Climate Dynamics, 5 July 18

Abstract

ENSO variability has a seasonal phase-locking, with SST anomalies on average decreasing during the beginning of the year and SST anomalies increasing during the second half of the year. As a result of this, the ENSO SST variability is smallest in April and the so call 'spring barrier' exists in the predictability of ENSO. In this study we analysis how the seasonal phase-locking of surface short wave radiation associated with cloud cover feedbacks contribute to this phenomenon. We base our analysis on observations and simplified climate model simulations. At the beginning of the year, the warmer mean SST in the eastern equatorial Pacific leads to deeper clouds whose anomalous variability are positively correlated with the underlying SST anomalies. These observations highlight a strong negative surface short wave radiation feedback at the beginning of the year in the eastern Pacific (NINO3 region). This supports the observed seasonal phase-locking of ENSO SST variability. This relation also exists in model simulations of the linear recharge oscillator and in the slab ocean model coupled to a fully complex atmospheric GCM. The Slab ocean simulation has seasonal phase-locking similar to observed mostly caused by similar seasonal changing cloud feedbacks as observed. In the linear recharge oscillator simulations seasonal phase-locking is also similar to observed, but is not just related to seasonal changing cloud feedbacks, but is also related to changes in the sensitivity of the zonal wind stress and to a lesser extent to seasonally change sensitivities to the thermocline depth. In summary this study has shown that the seasonal phase-locking, as observed and simulated, is linked to seasonally changing cloud feedbacks.

1. Introduction

The El Nino Southern Oscillation (ENSO) variability is the leading mode of interannual climate variability. It is marked by a pattern of sea surface temperature (SST) anomalies in the tropical Pacific with largest amplitudes in the central to eastern equatorial Pacific. The SST variability tends to be strongest in boreal winter and weakest in boreal spring. This seasonal phase-locking is an important characteristic of ENSO, as it indicates that the underlying dynamics controlling the evolution of this mode are state dependent. It is also important for predicting the evolution of ENSO, as only models that can simulate the seasonal phase-locking and the associated 'spring barrier' correctly are able to simulate the growth and decay of SST anomalies adequately. The correct phase locking is also important for the correct simulation of the ENSO teleconnections, as many teleconnections display strong seasonal phase-locking too.

A realistic seasonal phase-locking of ENSO is still a significant challenge for most state-of-the-art Coupled General Circulation Models (CGCMs) [e.g. Bellenger et al., 2014 and Rashid and Hirst, 2015]. Models from the Coupled Model Inter-comparison Project (CMIP) version 3 and 5 have significant problems in simulating the right seasonality of ENSO in both, the seasonal phase and in its amplitude. Rashid and Hirst [2015] found that the biases in the cloud simulations are key in controlling the ENSO phase-locking biases in the ACCESS model simulations.

The dynamics that cause the seasonal phase-locking are yet not fully understood, although it has been studied in a number publications [e.g. Chang et al., 1995, Tziperman et al., 1995, Jin et al., 1996, Harrison and Vecchi, 1999, Neelin et al., 2000, Stein et al. 2010, Stuecker et al., 2013, McGregor et al., 2013, Ham et al., 2013, Levine and McPhaden, 2015 or Zhu et al., 2015]. Most of these studies discuss the ENSO phase-locking in the context of stochastic chaos theory, but do not address, which physical process of the seasonal cycle do cause the ENSO phase locking. Harrison and Vecchi [1999], Stuecker et al. [2013] and McGregor et al. [2012, 2013] argue that the southward wind shift or second mode of zonal wind stresses is causing the termination of ENSO in the spring season. Thus they argue that seasonally changing sensitivities in the zonal wind is leading to the ENSO phase-locking. Zhu et al. [2015] found that the thermocline-SST feedbacks may be one of the causes for ENSO spring persistence barrier. Stein et al. [2010] and Levine and McPhaden [2015] both analysed the seasonality in the growth rate of the recharge oscillator model and found that this is able to explain the spring barrier.

In general ENSO dynamics are a result of different processes interacting [e.g. BJERKNES, 1969, Jin, 1997, Neelin et al., 1998 or Dommenget, 2010]. These include oceanic, atmospheric and coupled processes. The main interactions between the zonal wind stress, SST and the thermocline depth which create anomaly growth are often summarized as the Bjerknes feedbacks [BJERKNES, 1969]. The simple Recharge Oscillator (ReOsc) model of Jin (1997) combines these growth mechanisms with mechanisms for the anomaly decay. This model has been further simplified by Burgers et al. [2005], which describes ENSO as a recharge and discharge of heat content along the whole equatorial Pacific forced by zonal wind stress in the central equatorial Pacific and atmospheric heat fluxes over the NINO3 region (5^{o}S to 5^{o}N / 150^{o}W to 90^{o}W).

The ReOsc model coupled to a fully complex atmosphere model has been used to study ENSO dynamics by Frauen and Dommenget [2010] and by Yu et al. [2015]. Both studies found that realistic seasonal ENSO phase-locking exists in the ReOsc model simulations. In both model simulations the ocean dynamics are linearized with constant (seasonally not changing) model parameters. Thus, indicating that the seasonality of ENSO in these simulations results entirely from the atmospheric zonal wind stress and heat fluxes. Yu et al. [2015] also found SST variability with the same seasonal phase-locking as the observed ENSO in a configuration of the model which included only a Slab Ocean with constant 50m depth (i.e., no upper ocean dynamics). In this simulation seasonality of SST variability results entirely from atmospheric heat fluxes only. Thus these simplified models of tropical SST variability suggest that realistic ENSO seasonal phase-locking can result from atmospheric processes only.

The ENSO dynamics have also been analysed in the context of cloud feedbacks [e.g. Barnett et al., 1991, Waliser et al., 1994, Wang and McPhaden, 2000 or Guilyardi et al., 2009]. It is in general argued that surface short wave cloud feedbacks tend to dampen the ENSO variability. However, in some situations they can be positive feedbacks too [e.g. Dommenget et al., 2014]. Dommenget et al. [2014] argue that the cloud feedbacks are SST state dependent, with warmer SSTs favouring negative cloud surface short wave feedbacks and colder SSTs favour more positive cloud feedbacks. The role that cloud feedbacks play in the context of the seasonal phase-locking have so far not been addressed.

The aim of this study here is to analyse the relationship between ENSO seasonal phase-locking and the seasonally changing cloud cover feedbacks in observations and in simplified model simulations. We will illustrate that cloud cover feedbacks change seasonally in a way that supports the observed seasonal phase-locking of ENSO. We will also illustrate that in some simplified coupled model simulations the seasonally changing cloud cover feedbacks are the main cause of the ENSO seasonal phase-locking.

The paper is organized as follows: The following section describes datasets and the model simulations used in this study. In section 3 we analyse the observed seasonal phase-locking and its relation to cloud cover feedbacks. In section 4 and 5 we illustrate the seasonal phase-locking in the slab ocean and the ReOsc model simulations. The study is concluded with a summary and discussion.

2. Observations, Models and Methods

Observed SSTs are based on the HADISST dataset from 1870 to 2011 [Rayner et al., 2003]. Cloud cover observations from 1984 to 2002 are taken from the ISCCP dataset [Rossow and Schiffer, 1999]. The NCEP reanalysis [Kalnay et al., 1996] cloud cover or short wave surface radiation are not used in this study. Cloud cover observations are not assimilated into the NCEP reanalysis and the cloud cover variability in the ISCCP and NCEP dataset appear to be significantly different from each other. The ISCCP observations are therefore preferred.

In this study three different hybrid coupled GCM model simulations are studied that all use the same atmospheric GCM model, but differ only in the formulation of the simplified ocean models. These are the same model simulations studied in Yu et al. [2015]. The main elements of the model simulations are presented below, but for details on the model development see Yu et al. [2015]. The

atmospheric GCM in all three simulations is a low-resolution version (3.75° x 2.5°) of the Australian Community Climate and Earth System Simulator (ACCESS) model of the UK Meteorological Office Unified Model AGCM with HadGEM2 physics [Davies et al., 2005, Martin et al., 2010, Martin et al., 2011 and Bi et al., 2013]. In all three simulations the ocean is simulated with simplified models and SST climatologies are forced to be similar to the observed by either prescribing the mean SST or by flux corrections.

The first ocean model is a Slab Ocean model with constant mixed layer depth of 50m:

$$\gamma \frac{dSST(\vec{x},t)}{dt} = F_{atmos}(\vec{x},t) + F_Q(\vec{x},t_j) \qquad [1]$$

Where γ is the heat capacity of the 50m mixed layer and F_{atmos} is the net heat flux into the ocean. The flux correction, F_Q, is a state-independent flux correction that forces the model to have the same mean SST climatology as observed. Both SST and F_{atmos} are functions of location, $\vec{x}$, and time, t, and F_Q is a function of location and calendar day of the year, t_j. Thus this SST tendency eq. [3] models the SST at every grid point for each time step. We refer to this model as the Slab simulation.

The second ocean model utilises the slab ocean component outside of the tropical Pacific (20°S–20°N, 130°E–70°W), while within the tropical Pacific region SSTAs are calculated with the low order 2-dimensional recharge oscillator toy model similar to Frauen and Dommenget [2010] (the model is referred to as ReOsc). The ReOsc toy model from Burgers et al. [2005] is given by two coupled differential equations of SST anomalies in the NINO3 region, T, and the thermocline depth anomalies over the whole equatorial Pacific, h:

$$\frac{dT(t)}{dt} = a_{11}T(t) + a_{12}h(t) + \zeta_1 \qquad [2]$$

$$\frac{dh(t)}{dt} = a_{21}T(t) + a_{22}h(t) + \zeta_2 \qquad [3]$$

The two equations are forced by stochastic noise terms ζ_1 and ζ_2. The model parameters a_{11} and a_{22} represent the damping (or growth rate) of T and h, and the parameters a_{12} and a_{21} the coupling between T and h. In the ReOsc simulation eqs. [1] and [2] are coupled to the atmosphere model leading to the equations:

$$\frac{dT(t)}{dt} = a_{11O}T(t) + a_{12}h(t) + a_{12}\lambda\tau(t) + \frac{f(t)}{\gamma} \qquad [4]$$

$$\frac{dh(t)}{dt} = a_{21O}T(t) + a_{22}h(t) + \frac{\lambda}{2}a_{22}\tau(t) \qquad [5]$$

where f is the averaged F_{atmos} anomaly in NINO3 region and τ is averaged zonal wind stress anomaly in the central Pacific (6°S–6°N, 160°E–140°W). λ is a free coupling parameter that is tuned in sever iterations as done in Frauen and Dommenget [2010]. a_{11O} and a_{21O} are the residuals of the original parameters a_{11} and a_{21} that exclude the linear relation to τ and f with T from atmospheric feedbacks with regression coefficients $C_{\tau T}$ and C_{fT}, respectively. Thus a_{11O} and

a_{21O} represent the oceanic feedbacks to the tendencies to T as function of T and h. The atmospheric feedbacks are included in f and τ, which also include the atmospheric stochastic forcings.

As the ReOsc model only represents temperatures in the NINO3 region, anomalies of tropical Pacific temperature were generated by multiplying the modelled NINO3 anomalies with the pattern of the recharge oscillator component, $P_{ReOsc}(\vec{x})$ (see Yu et al. [2015]) . The SST climatology of the Slab model, $SST_{clim}(\vec{x}, t_j)$, was added before coupling with the atmosphere:

$$SST(\vec{x}, t) = SST_{clim}(\vec{x}, t_j) + T(t) \cdot P_{ReOsc}(\vec{x}) \qquad [6]$$

The third ocean model (referred to as ReOsc-Slab) considers both Slab Ocean eq. [3] and the ReOsc model eqs. [4-6] in the tropical Pacific (20°S–20°N, 130°E–70°W) leading to the SST equations:

$$\gamma \frac{dSST(\vec{x},t)}{dt} = F_{atmos}(\vec{x}, t) + F_Q(\vec{x}, t_j) + P_{ReOsc}(\vec{x}) \cdot [a_{11O}T(t) + a_{12}h(t) + a_{12}\lambda\tau(t)] \cdot \gamma^{-1} \qquad [7]$$

Each of the three model simulations is 500yrs long. The model parameters ($\gamma, \lambda, a_{11O}, a_{21O}, a_{12}, a_{22}, C_{\tau T}$ and C_{fT}) of all three simulations are constants without any seasonal cycle, see Table 1. Thus all seasonal changing characteristics in these three simulations must result from seasonal changes in the characteristics of F_{atmos} (in the Slab Ocean and ReOsc-Slab simulation) or from f and τ (in the ReOsc and ReOsc-Slab simulation).

The ReOsc model eqs. [2] and [3] can also be used to estimate the model parameters from observed or simulated T and h statistics [Burgers et al., 2005: Jansen et al., 2009]. The effective ReOsc parameters a_{11}, a_{12} , a_{21} and a_{22} are estimated for the model simulations statistics by multivariate linear regression. The model parameters of eqs. [4-7] and the statistical sets of the parameter do not need to be the same and in general will not be the same due the interaction of different processes and due to the atmospheric forcings not simply being a linear function of the NINO3 SST. The parameters of eqs. [4-7] are by construction constants without any seasonal cycle. The effective estimates of the ReOsc toy model parameters (eqs. [2] and [3]) based on the regression on the T and h statistics from the ReOsc simulation can be seasonally changing. The effective statistical ReOsc parameters a_{11}, a_{12}, a_{21} and a_{22} are estimated for each calendar month.

All analyses presented here are based on monthly mean data, with the anomalies defined for each data set or model simulation individually relative to the data or models mean seasonal climatology. Seasonal lag-lead correlations are based on monthly data, with comparing a particular calendar month of the first variable (presented on the y-axis in the figures) with the lag/lead month of the second variable. The calendar month of the other variable is relative to the first variable (e.g. for calendar month 7 in the first variable a lag of +3 refers to calendar month 4 in the second variable).

3. Observed seasonal phase-locking

The observed SST standard deviation in the NINO3 region (150°W to 90°W/5°S to 5°N) is strongest in boreal winter (November to Jan) and weakest in boreal spring (March to April), see Fig. 1. Thus SST anomalies tend to decrease in amplitude, in average, from December to April and in turn SST anomalies tend to grow in amplitude, in average, from April to December. These different average tendencies at different parts of the calendar year can be illustrated by the lag-lead correlation between the SST and its tendencies (derivative) as a function of calendar month, see Fig. 2. The average, over all months, lag-lead correlation between the SST and SST tendencies (black line in Fig. 2a) is asymmetric around zero lag, with positive SST tendencies leading the SST evolution, zero cross correlation at zero lag and negative SST tendencies lagging the SST. This is illustrating that in average the SST tendencies build up the SST anomalies as much as they decrease them after the SST peak. However, focusing on individual calendar months, this lag-lead relation is not equally balanced around zero lag. In October (red line in Fig. 2a), for instance, the SST tendencies have a positive correlation at lag zero and for SST leading the SST tendencies. This illustrates that SST anomalies are in average still increasing in October. In turn, in February the SST tendencies are negative at lag zero and even when the SST tendencies are leading, indicating that SST anomalies are in average decreasing in February. The complete picture is shown in Fig. 2b. We can see that at the beginning of the year the SST tendencies are more negative and in the later half of the year the SST tendencies are mostly positive.

The different tendencies at different seasons of the year indicate state dependent feedbacks and forcings. As discussed in the introduction, ENSO has a number of processes influencing the feedbacks and forcings and thus the SST tendencies. It is beyond the scope of this study to analyse all elements of the ENSO dynamics, but we shall focus here on the role of the cloud feedback. A starting point to understand the seasonal changes in the cloud feedbacks is the mean SST climatology along the equatorial Pacific (Fig. 3a). The beginning of the year marks the warmest season in the central to eastern equatorial Pacific SSTs. It is during this season that the SSTs are warm enough to allow deep convection and the associated deeper and higher clouds. This is reflected in the mean cloud cover, which increases during the warm season (Fig. 3b). Most importantly the cloud feedback is increasing substantially, which is illustrated in Fig. 3c by the linear regression of the total cloud cover with the underlying SST. In particular over the NINO3 region we see a very clear change in the linear regression between cloud cover and SST, see Fig. 4a. At the beginning of the year we have strong regression with more than 10% total cloud cover change per degree SST anomaly along the equator. In the later half of the year, however, total cloud cover is almost independent of the SST anomalies for most of the eastern equatorial Pacific. This is consistent with the state dependent cloud feedbacks discussed in Dommenget et al. [2014].

This seasonality suggests a stronger negative surface short wave cloud feedback in the beginning of the year: positive SST anomalies are counteracted by stronger negative surface short wave flux anomalies. We can roughly estimate the strength of a linear cloud feedback in the NINO3 region SSTAs with the strength of the linear regression coefficient between cloud cover and SST in the NINO3

region, r_{sst}, (Fig. 4a) and by assuming a short wave cloud albedo of about $\alpha_{cloud} = 0.5$. The linear damping by SST can then be written as:

$$F_{cloud} = -r_{sst}(t_j) \cdot \alpha_{cloud} \cdot S_{or}(t_j) \cdot T \quad [8]$$

with $S_{or}(t_j)$as the incoming solar radiation (constant 420W/m^2). F_{cloud} is shown in Fig. 4b. The strength of the surface short wave cloud feedback in the NINO3 region is changing from about $-30\frac{W}{m^2K}$ in March to about $-2\frac{W}{m^2K}$ in November (Fig. 4b). The values are on average similar to the short wave surface radiation feedbacks values found in Bellenger et al. [2014]. We can illustrate that such a seasonally changing cloud surface short wave feedback can lead to seasonally phase-locking of SST with similar timing to that observed. For this we consider the simple toy model:

$$\gamma \frac{dT}{dt} = -c \cdot T + F_{cloud} + F_{noise} \quad [9]$$

Here the heat capacity, γ, is assumed be that of a 20m mixed layer, which is about the average mixed layer depth in the NINO3 region Lorbacher et al. [2006]. The linear damping independent of the cloud cover, c = -7.4W/m^2, which results into a net average linear damping of about -17W/m^2. This value is similar to that estimate for observations in Bellenger et al. [2014]. The SST standard deviation of the model in eq. [9] integrated with a time step on one day over 10^4 years and noise forcing of 100W/m^2 is shown in Fig. 4c. Qualitatively the seasonal phase-locking of the SST in the simple toy model is similar to that observed, with minimum SST variability in April and increasing SST variability to later half of the year by about 50%.

4. Slab Ocean seasonal phase locking

We now take a look at the seasonal phase-looking in the Slab Ocean coupled simulation. In Fig. 1 we can see that the seasonal phase-looking of SST variability is qualitatively similar to that observed, but the overall variability is weaker than observed. The cross-correlation between SST and the SST tendencies over the different calendar months is also very similar to the observed, with negative tendencies dominating at the beginning of the year and positive tendencies dominating in the middle and the later half of the year (Fig. 5a). In the Slab Ocean model the SST tendencies are directly proportional to the net atmospheric heat fluxes, F_{atmos}. Thus the same cross-correlation is found between F_{atmos} and SST, see Fig. 5d. This is different in the other two simulations (ReOsc and ReOsc-Slab), in which SST tendencies are not solely forced by F_{atmos} and subsequently the cross-correlation between F_{atmos} and SST is not the same as the cross-correlation between SST tendencies and SST.

In the coupled Slab Ocean simulation the SST tendencies are the sum of the four components of F_{atmos}: *short wave* (F_{SW}), *long wave* (F_{LW}), *sensible* (F_{sense}) and *latent* (F_{latent}). The cross-correlation of these four components with the SST is shown in Fig. 6. This illustrates that the F_{SW} is the primary cause of the simulated seasonal phase-locking, as it closely matches the cross-correlation between SST-tendencies and SST (Fig. 5a). F_{LW}, is mostly counter acting F_{SW}, as expected since

both are related to cloud cover changes, but with mostly opposite heating effects. F_{latent} is dominated by negative cross-correlation with SST, indicating that it is mostly damping the SST variability through out the whole year with an exception around March to June, where positive F_{latent} anomalies lead the SST anomalies indicating it causes growth of SST variability in this part of the year. F_{sense} is also similar F_{SW} and to the observed seasonal phase-locking, indicating it also supports the observed seasonal phase-locking of SST anomalies. However, the amplitudes of F_{sense} anomalies are fairly small (not shown) and it is thus not important for the SST tendencies overall. In summary, we find that the seasonal phase-locking in the Slab Ocean is essentially caused by the seasonal changing F_{SW} forcings and thus it is caused by seasonal changes in the cloud cover feedbacks.

The seasonally changing short wave feedback along the equatorial Pacific in the Slab Ocean simulation is illustrated in Fig. 7a. In the first half of the year negative correlation of total cloud covers with SST dominates in the eastern Pacific, which represents a negative cloud surface short wave radiation feedback for the SST and is consistent with the picture discussed above (Fig. 6a). In the later half of the year the sign of the cross-correlation changes towards positive correlation, which indicates a more positive cloud short wave radiation feedback for the SST. This picture is roughly consistent with the observed seasonal changes in the cloud cover feedbacks (Fig. 3c). However, in the model simulation the positive correlation between short wave and SST in the eastern equatorial Pacific would correspond to a negative cloud cover vs. SST regression, which in observations is not as strong (in the far east; Fig. 3) or is actually still weakly positive (in parts of the eastern Pacific; Fig. 3). It is also consistent with the picture that during warmer SSTs (see Fig. 3a) the cloud cover is in a deep convection regime and in that it leads to negative cloud surface short wave radiation feedbacks, thus representing a state-dependent cloud feedback [Dommenget et al., 2014].

5. Recharge Oscillator seasonal phase locking

The seasonal phase-locking of the SST in the ReOsc model is also similar to observed and similar to that in the Slab Ocean model (Fig. 1 and 5b). However, the dynamics causing this similarity to the observed phase-locking are different from that in the Slab Ocean simulation, despite both utilising the same atmospheric model. The difference results from the different underlying SST equations of the ReOsc simulation compared to the Slab Ocean model (see model section 2). In the ReOsc model the SST tendencies (eq. [4]) are forced by four different terms related to temperature, wind stress, thermocline depth and net heat flux. The relative seasonal damping (or growth rate) effect of the different terms in eq. [4] can be illustrated by the linear regression of the net heat flux, wind stress and thermocline depth onto the NINO3 SST anomalies, see Fig. 8. Here each regression is scaled by its contribution to eq. [4] for better relative comparison.

The net heat flux is damping through out the whole year, but the damping is strongest in boreal spring and weakest in the later half of the year. This is similar to the Slab model simulation and is consistent with the lag zero cross-correlation between net heat and SST shown in Fig. 5e. Again we find that the short wave is damping at the beginning of the year and amplifying in the later half of the year

(Fig. 6e). The correlation between short wave radiation and SST along the equator is also similar to that in the Slab Ocean simulation (Fig. 7b).

The wind stress has a net growing tendency for the SST throughout the year, but it is weakest at the beginning of the year and strongest in the middle of the year. This also supports the seasonal phase-locking of the SST evolution. The thermocline depth has damping tendencies for the SST at the beginning and end of the year and growing tendencies in the middle of the year. This also supports the right seasonal phase-locking of the SST evolution, although shift to slightly earlier in the year and even starting at the end of the calendar year. In the classical picture of ENSO it is the thermocline depth that drives the SST evolution and the atmospheric heat flux is damping. This picture is also valid in the ReOsc simulation, where the net heat flux is mostly damping the SST evolution. The thermocline depth has the out of phase seasonal cross-correlation with SST that is consistent with a driving force (Fig. 9). Thus in the ReOsc simulation the thermocline depth is mostly the driving force of the SST evolution and the net heat flux is mostly a damping.

The relative importance of the three different forcing terms in causing the seasonal phase-locking can be evaluated by the amplitude of the seasonal changes in Fig. 8 as each of the terms shown in Fig. 8 was scaled by the parameters in the equivalent terms of eq. [4]. The wind stress and the net heat flux have similarly large contributions to the seasonality, whereas the thermocline depth contributes slightly less. Thus the seasonality in the ReOsc model is a combination of the seasonally changing sensitivities to wind stress, net heat flux (mostly due to the short wave) and the thermocline depth.

The seasonality in the dynamics of the ReOsc simulation can also be well captured in the seasonality of the effective ReOsc model parameters (Fig. 10a; see methods section for details) following the approach of Burgers et al. [2005] and Frauen and Dommenget [2010]. The seasonality of all four effective ReOsc parameters and of the two forcing terms estimated over the 500yrs of the ReOsc simulations are shown in Fig. 10a. We can note that the only significant seasonality exist in the damping of the SST. All other parameters, including the noise forcing terms, have very little seasonality. The effective seasonality in a_{11} is consistent with the combined effect of the three forcing terms shown in Fig. 8 and the remaining SST damping term with a_{110} in eq. [4].

We can integrate the ReOsc toy model eqs. [2] and [3] with the effective seasonal parameters as shown in Fig 10a and with random white noise forcing terms to illustrate how the seasonality of the SST would be according to the effective seasonal parameters. The seasonal phase locking of the seasonal ReOsc toy model is essentially the same as the ReOsc simulation (Fig 10b). If we integrate the toy model again with all effective seasonal parameters, but with the annual mean value of the effective a_{11} parameter (blue line in Fig. 10b), then the SST seasonal phase locking is essentially not present. In turn if we integrate the toy model again with the annual mean values of all the effective parameters and only the effective seasonal a_{11} parameter (red line in Fig. 10b), then the SST seasonal phase locking is essentially the same as in the complete seasonal toy model. Thus the damping or growth rate of the ReOsc model (a_{11}) is the main parameter causing the seasonality in the ReOsc simulation. Similar results were also found by Stein et al. [2010] and Levine and McPhaden [2015] by analysing the recharge oscillator fitted to observed data.

The ReOsc-Slab simulation combines the ReOsc and Slab model equations, and the resulting SST variability is a non-linear interaction between the two model equations as discussed in Yu et al. [2015]. The SST variability is larger than in the Slab and ReOsc simulation indicating that the interaction between the two is enhancing the SST variability (Fig. 1). It is also large than would be expected from a linear superposition of two independent sources of SST variability as discussed in Yu et al. [2015].

It is very similar to the ReOsc simulation in all seasonal phase-locking characteristics discussed above. A noticeable difference is that the seasonal phase-locking is shifted by about a month or two. This is related to the shift in the seasonal growth rate and damping in the wind stress and thermocline forcing (Fig. 8b and c). The surface short wave cloud feedbacks are qualitatively the same as in the ReOsc and Slab ocean only simulations. In summary, the ReOsc-Slab simulations suggest that the combine SST variability of ReOsc and Slab ocean dynamics are essentially similar to the ReOsc simulation, but the non-linear interactions complicate the dynamics slightly.

6. Summary and Discussion

In this study we examined the role of surface short wave cloud feedbacks in the seasonal phase-locking of ENSO. We analysed observed total cloud cover and three different hybrid coupled GCM model simulations with simplified ocean models. The simplified ocean models included a slab ocean model, a recharge oscillator model and a model that combines the slab and recharge oscillator equations. The simplified models have the advantage that the interactions causing the ENSO SST variability are strongly simplified and in the case of the slab ocean model simulation are just a result of surface heat flux forcings.

The observed relationship between total cloud cover and SST along the equatorial Pacific has a pronounce seasonal cycle, with a strong positive correlation between SST and total cloud cover in the eastern part of the equatorial Pacific at the first half of the year and nearly no or a negative correlation in the later half of the year. The strong positive correlation between SST and total cloud cover falls into the warm season of the eastern equatorial Pacific, which is also marked by more total cloud cover and by a deep cloud cover regime in contrast to the cold seasons in which shallower clouds are dominant. This is consistent with the SST state-dependent cloud feedbacks described in Dommenget et al. [2014].

A simple estimate of the surface short wave effect of the seasonal correlation between total cloud cover and SST suggests that the damping by surface short wave will be strongest in March and weakest in the second half of the year. An integration of a simple mixed layer heat budget equation suggests that such a seasonal changing short wave feedback could lead to seasonal phase-locking that is qualitatively similar to that observed. However, it should be noted that here we only considered the effect of cloud surface short wave feedbacks, neglecting the effect of total cloud cover on surface long wave feedbacks and how clouds may affect the radiation budget within the higher levels of the atmosphere. The surface long wave radiation will in general have compensating effects. It is beyond the scope of this study to discuss all elements of seasonal feedbacks or other cloud related feedbacks. This needs to be addressed in future studies.

The Slab ocean simulations showed a seasonal phase-locking in NINO3 SST variability that is qualitatively similar to observed, albeit with a reduced amplitude. This as such is interesting as this model is entirely driven by atmospheric heat fluxes only. The analysis of the heat flux components in the Slab simulation revealed that the surface short wave heat fluxes are the dominant contributor of this modelled seasonal phase-locking. This in turn indicates that the total cloud cover short wave feedbacks in the Slab simulation are the main driver of the seasonal phase-locking. The Slab, ReOsc and ReOsc-Slab simulations all have seasonally changing correlation between SST and surface short wave along the equatorial eastern Pacific that are supporting the observed seasonal phase-locking of ENSO.

In the ReOsc and the ReOsc-Slab simulations the seasonal phase-locking is more complicated than in the Slab simulations and is not only caused by seasonally changing surface short wave cloud feedbacks. In the ReOsc simulation the essential seasonality is in the damping or growth rate (a_{11} parameter) of the recharge oscillator model (eq. [2]), as it was also found by Stein et al. [2010] and Levine and McPhaden [2015]. This seasonally changing damping or growth rate results from three factors, i) the seasonally changing net heat flux damping (mostly the short wave), ii) the zonal wind stress sensitivity, and iii) slightly less from the thermocline depth forcing.

In the real observed ENSO the interactions leading to the seasonal phase-locking are likely to be more complicated than found in the simplified models used here, as more processes are involved in the ENSO dynamics that are not considered here. A good example for this is the mechanism described by Harrison and Vecchi [1999] and McGregor et al. [2013]. They found that the discharging of equatorial warm water volume (changes in zonal mean thermocline depth) related to meridional shift of zonal wind is causing the spring termination of ENSO events. This mechanism is not explicitly simulated in the simplified simulations discussed here. Thus it seems that a number of processes in the ocean and atmosphere are contributing to the seasonal phase-locking of ENSO, but this study emphasizes the potentially prominent role of cloud feedbacks which had not been considered previously.

The importance of seasonally changing cloud feedbacks in controlling the ENSO seasonal phase-locking may have some important implication for CGCM simulations. Current state of the art CGCM in the CMIP5 database have substantial problems in simulating the observed cloud feedbacks [e.g. Bellenger et al., 2014 or Dommenget et al., 2014]. They also have still significant problems in simulating the right seasonal phase-locking of ENSO, which at least in the ACCESS model appear to be related to the simulations of the clouds [Rashid and Hirst, 2015]. Much of these cloud and seasonal phase-locking problems are likely be related to biases in the SST cold tongue. Improving the representation of cloud feedbacks in the tropical Pacific will most likely lead to a substantial improvement in the seasonal phase-locking of ENSO.

Acknowledgments

We like to thank Shayne McGregor, Harun Rashid, Axel Timmerman and the ENSO workshops in Sydney and Paris 2015 for fruitful discussions and comments. This study was supported by the ARC project “Beyond the linear

dynamics of the El Nino Southern Oscillation" (DP120101442) and the ARC Centre of Excellence for Climate System Science (CE110001028). The experiments were performed on the NCI National Facility in Canberra, Australia, which is supported by the Australian Commonwealth Government.

References

Barnett, T. P., M. Latif, E. Kirk, and E. Roeckner, 1991: On Enso Physics. *Journal of Climate*, **4,** 487-515.

Bellenger, H., E. Guilyardi, J. Leloup, M. Lengaigne, and J. Vialard, 2014: ENSO representation in climate models: from CMIP3 to CMIP5. *Climate Dynamics*, **42,** 1999-2018.

Bi, D. H., M. Dix, S. J. Marsland, S. O'Farrell, H. A. Rashid, P. Uotila, A. C. Hirst, E. Kowalczyk, M. Golebiewski, A. Sullivan, H. L. Yan, N. Hannah, C. Franklin, Z. A. Sun, P. Vohralik, I. Watterson, X. B. Zhou, R. Fiedler, M. Collier, Y. M. Ma, J. Noonan, L. Stevens, P. Uhe, H. Y. Zhu, S. M. Griffies, R. Hill, C. Harris, and K. Puri, 2013: The ACCESS coupled model: description, control climate and evaluation. *Australian Meteorological and Oceanographic Journal*, **63,** 41-64.

BJERKNES, J., 1969: ATMOSPHERIC TELECONNECTIONS FROM THE EQUATORIAL PACIFIC. *Mon. Wea. Rev.*, **97,** 163–172.

Burgers, G., F. F. Jin, and G. J. van Oldenborgh, 2005: The simplest ENSO recharge oscillator. *Geophysical Research Letters*, **32,** -.

Chang, P., L. Ji, B. Wang, and T. Li, 1995: Interactions between the Seasonal Cycle and El-Nino Southern-Oscillation in an Intermediate Coupled Ocean-Atmosphere Model. *Journal of the Atmospheric Sciences*, **52,** 2353-2372.

Davies, T., M. J. P. Cullen, A. J. Malcolm, M. H. Mawson, A. Staniforth, A. A. White, and N. Wood, 2005: A new dynamical core for the Met Office's global and regional modelling of the atmosphere. *Quarterly Journal of the Royal Meteorological Society*, **131,** 1759-1782.

Dommenget, D., 2010: The slab ocean El Nino. *Geophysical Research Letters*, **37,** -.

Dommenget, D., S. Haase, T. Bayr, and C. Frauen, 2014: Analysis of the Slab Ocean El Nino atmospheric feedbacks in observed and simulated ENSO dynamics. *Climate Dynamics*, **42,** 3187-3205.

Frauen, C. and D. Dommenget, 2010: El Nino and La Nina amplitude asymmetry caused by atmospheric feedbacks. *Geophysical Research Letters*, **37,** -.

Guilyardi, E., P. Braconnot, F. F. Jin, S. T. Kim, M. Kolasinski, T. Li, and I. Musat, 2009: Atmosphere Feedbacks during ENSO in a Coupled GCM with a Modified Atmospheric Convection Scheme. *Journal of Climate*, **22,** 5698-5718.

Ham, Y. G., J. S. Kug, D. Kim, Y. H. Kim, and D. H. Kim, 2013: What controls phase-locking of ENSO to boreal winter in coupled GCMs? *Climate Dynamics*, **40,** 1551-1568.

Harrison, D. E. and G. A. Vecchi, 1999: On the termination of El Nino. *Geophysical Research Letters*, **26,** 1593-1596.

Jansen, M. F., D. Dommenget, and N. Keenlyside, 2009: Tropical Atmosphere-Ocean Interactions in a Conceptual Framework. *Journal of Climate*, **22,** 550-567.

559 Jin, F. F., 1997: An equatorial ocean recharge paradigm for ENSO .1. Conceptual
560 model. *Journal of the Atmospheric Sciences*, **54,** 811-829.

561 Jin, F. F., J. D. Neelin, and M. Ghil, 1996: El Nino Southern Oscillation and the
562 annual cycle: Subharmonic frequency-locking and aperiodicity. *Physica*
563 *D*, **98,** 442-465.

564 Kalnay, E., M. Kanamitsu, R. Kistler, W. Collins, D. Deaven, L. Gandin, M. Iredell, S.
565 Saha, G. White, J. Woollen, Y. Zhu, M. Chelliah, W. Ebisuzaki, W. Higgins, J.
566 Janowiak, K. C. Mo, C. Ropelewski, J. Wang, A. Leetmaa, R. Reynolds, R.
567 Jenne, and D. Joseph, 1996: The NCEP/NCAR 40-year reanalysis project.
568 *Bulletin of the American Meteorological Society*, **77,** 437-471.

569 Levine, A. F. Z. and M. J. McPhaden, 2015: The annual cycle in ENSO growth rate
570 as a cause of the spring predictability barrier. *Geophysical Research*
571 *Letters*, **42,** 5034-5041.

572 Lorbacher, K., D. Dommenget, P. P. Niiler, and A. Kohl, 2006: Ocean mixed layer
573 depth: A subsurface proxy of ocean-atmosphere variability. *Journal of*
574 *Geophysical Research-Oceans*, **111,** -.

575 Martin, G. M., S. F. Milton, C. A. Senior, M. E. Brooks, S. Ineson, T. Reichler, and J.
576 Kim, 2010: Analysis and Reduction of Systematic Errors through a
577 Seamless Approach to Modeling Weather and Climate. *Journal of Climate*,
578 **23,** 5933-5957.

579 Martin, G. M., N. Bellouin, W. J. Collins, I. D. Culverwell, P. R. Halloran, S. C.
580 Hardiman, T. J. Hinton, C. D. Jones, R. E. McDonald, A. J. McLaren, F. M.
581 O'Connor, M. J. Roberts, J. M. Rodriguez, S. Woodward, M. J. Best, M. E.
582 Brooks, A. R. Brown, N. Butchart, C. Dearden, S. H. Derbyshire, I. Dharssi,
583 M. Doutriaux-Boucher, J. M. Edwards, P. D. Falloon, N. Gedney, L. J. Gray,
584 H. T. Hewitt, M. Hobson, M. R. Huddleston, J. Hughes, S. Ineson, W. J.
585 Ingram, P. M. James, T. C. Johns, C. E. Johnson, A. Jones, C. P. Jones, M. M.
586 Joshi, A. B. Keen, S. Liddicoat, A. P. Lock, A. V. Maidens, J. C. Manners, S. F.
587 Milton, J. G. L. Rae, J. K. Ridley, A. Sellar, C. A. Senior, I. J. Totterdell, A.
588 Verhoef, P. L. Vidale, A. Wiltshire, and H. D. Team, 2011: The HadGEM2
589 family of Met Office Unified Model climate configurations. *Geoscientific*
590 *Model Development*, **4,** 723-757.

591 McGregor, S., N. Ramesh, P. Spence, M. H. England, M. J. McPhaden, and A.
592 Santoso, 2013: Meridional movement of wind anomalies during ENSO
593 events and their role in event termination. *Geophysical Research Letters*,
594 **40,** 749-754.

595 Neelin, J. D., F. F. Jin, and H. H. Syu, 2000: Variations in ENSO phase locking.
596 *Journal of Climate*, **13,** 2570-2590.

597 Neelin, J. D., D. S. Battisti, A. C. Hirst, F. F. Jin, Y. Wakata, T. Yamagata, and S. E.
598 Zebiak, 1998: ENSO theory. *Journal of Geophysical Research-Oceans*, **103,**
599 14261-14290.

600 Rashid, H. A. and A. C. Hirst, 2015: Investigating the mechanisms of seasonal
601 ENSO phase locking bias in the ACCESS coupled model. *Climate*
602 *Dynamics*.

603 Rayner, N. A., D. E. Parker, E. B. Horton, C. K. Folland, L. V. Alexander, D. P. Rowell,
604 E. C. Kent, and A. Kaplan, 2003: Global analyses of sea surface
605 temperature, sea ice, and night marine air temperature since the late
606 nineteenth century. *Journal of Geophysical Research-Atmospheres*, **108,** -.

607 Rossow, W. B. and R. A. Schiffer, 1999: Advances in understanding clouds from
608 ISCCP. *Bulletin of the American Meteorological Society*, **80,** 2261-2287.

609 Stein, K., N. Schneider, A. Timmermann, and F. F. Jin, 2010: Seasonal
610 Synchronization of ENSO Events in a Linear Stochastic Model. Journal of
611 Climate, 23, 5629-5643.

612 Stuecker, M. F., A. Timmermann, F. F. Jin, S. McGregor, and H. L. Ren, 2013: A
613 combination mode of the annual cycle and the El Nino/Southern
614 Oscillation. *Nature Geoscience*, **6,** 540-544.

615 Tziperman, E., M. A. Cane, and S. E. Zebiak, 1995: Irregularity and Locking to the
616 Seasonal Cycle in an Enso Prediction Model as Explained by the Quasi-
617 Periodicity Route to Chaos. *Journal of the Atmospheric Sciences*, **52,** 293-
618 306.

619 Waliser, D. E., B. Blanke, J. D. Neelin, and C. Gautier, 1994: Shortwave Feedbacks
620 and El-Nino-Southern-Oscillation - Forced Ocean and Coupled Ocean-
621 Atmosphere Experiments. *Journal of Geophysical Research-Oceans*, **99,**
622 25109-25125.

623 Wang, W. M. and M. J. McPhaden, 2000: The surface-layer heat balance in the
624 equatorial Pacific Ocean. Part II: Interannual variability. *Journal of*
625 *Physical Oceanography*, **30,** 2989-3008.

626 Yu, Y., D. Dommenget, C. Frauen, G. Wang, and S. Wales, 2015: ENSO dynamics
627 and diversity resulting from the recharge oscillator interacting with the
628 slab ocean. *Climate Dynamics*.

629 Zhu, J., A. Kumar, and B. Huang, 2015: The relationship between thermocline
630 depth and SST anomalies in the eastern equatorial Pacific: Seasonality
631 and decadal variations. *Geophysical Research Letters*.

632

633

634

Tables

$\gamma = 2.02 \cdot 10^8 \frac{J}{m^2 K}$
$\lambda = 2100$
a_{11O} =-0.536$\frac{1}{mon}$
a_{21O} =-1.027$\frac{m}{mon \cdot K}$
a_{12} =0.021$\frac{K}{mon \cdot m}$
a_{22} =-0.008$\frac{1}{mon}$
$C_{\tau T}$ =0.011$\frac{N}{m^2 K}$
C_{fT} =-11.223$\frac{W}{m^2 K}$

Table 1: Parameters of the ACCES model simulations Slab, ReOsc and ReOsc-Slab.

Figures

Figure 1.: NINO3 SST standard deviation versus calendar month for observations and different model simulations.

Figure 2.: Left: auto-correlation of NINO3 SST (dotted) and cross-correlations of NINO3 SST with the SST tendencies for all calendar month (black solid), February (blue) and October (red). Right: cross-correlations of NINO3 SST with the SST tendencies vs calendar month of SST. Positive lags indicate the SST is leading the SST tendencies and the calendar month is relative to the SST.

Figure 3.: (a) mean SST along the equator. (b) mean cloud cover. (c) regression of cloud cover on SST. Averaging is done from 5^{o}S to 5^{o}N.

Figure 4.: Simple cloud feedback model: (a) linear regression of total cloud cover to SST in the NNINO3 region (mean of the values shown in Fig. 3). (b) Linear atmospheric damping parameter. (c) SST standard deviation in the simple cloud feedback toy model. See text for details.

Figure 5.: Seasonal cross-correlations: upper row: between SST and SST tendencies. Lower row: between SST and net heat flux. First column for the Slab, second ReOsc and third for the ReOsc-Slab simulation. Positive lags indicate the SST is leading and the calendar month is relative to the SST.

Figure 6.: Seasonal cross-correlation between SST and the heat flux components, SW (first column), LW (second column), sensible heat (third column) and latent heat (last column) for the Slab Ocean (first row), ReOsc (second row) and the ReOsc-Slab simulation (last row). Positive lags indicate the SST leading the heat flux evolution.

Figure 7.: Seasonal cross-correlation between SST and short wave along the equator (5^{o}S – 5^{o}N) for the Slab Ocean (a), ReOsc (b) and the ReOsc-Slab simulation (c).

Figure 8.: Seasonal regressions in the ReOsc (blue lines) and ReOsc-Slab (green lines) simulations: NINO3 SST vs. net heat (a), zonal wind stress in the central Pacific vs. NINO3 SST (b) and thermocline depth vs. NINO3 SST (c). All regression values are scaled by the corresponding parameters in eq. [4] to have the same scale in terms of monthly SST tendencies per SST.

Figure 9.: Seasonal cross-correlation between thermocline depth and SST in the ReOsc (a) and ReOsc-Slab simulation (b). Positive lags indicate the SST leading the thermocline depth evolution and the calendar month is relative to the SST.

Figure 10.: (a) The effective seasonal recharge oscillator parameters (eqs.[1] and [2]) estimate from the ReOsc simulation. (b) Seasonally resolved NINO3 SST standard deviation of a Monte Carlo integration of the recharge oscillator

model (eqs.[1] and [2]) with different combinations of the effective seasonal parameters in (a). See text for details.

Figure 1

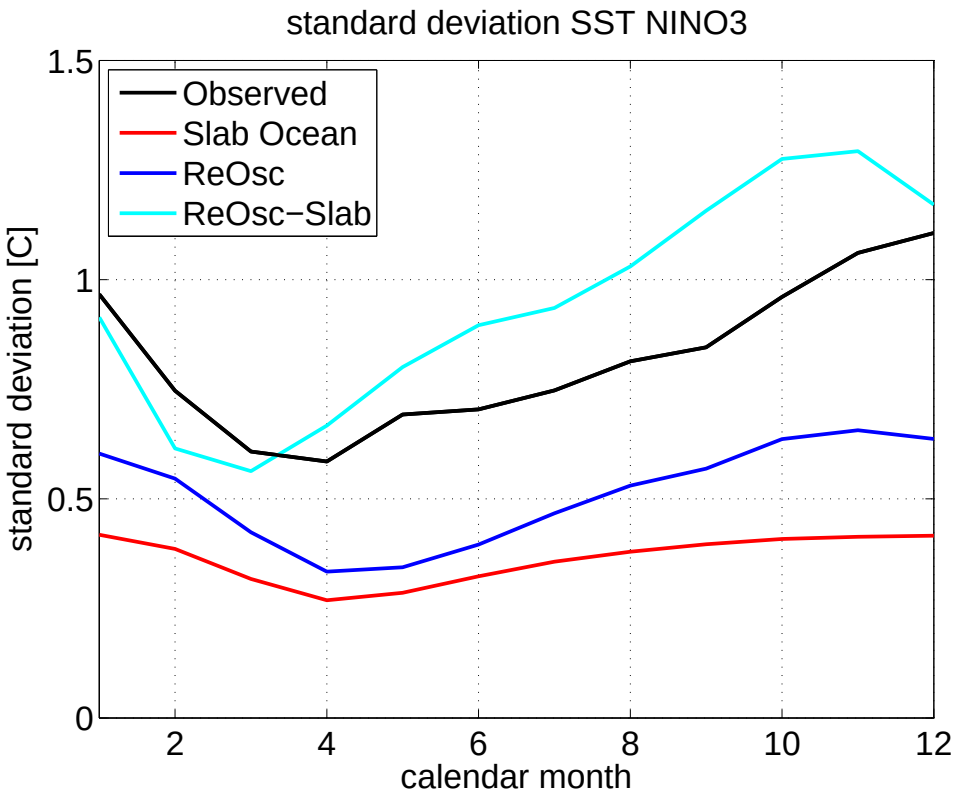

Figure 1: NINO3 SST standard deviation versus calendar month for observations and different model simulations.

Figure 2

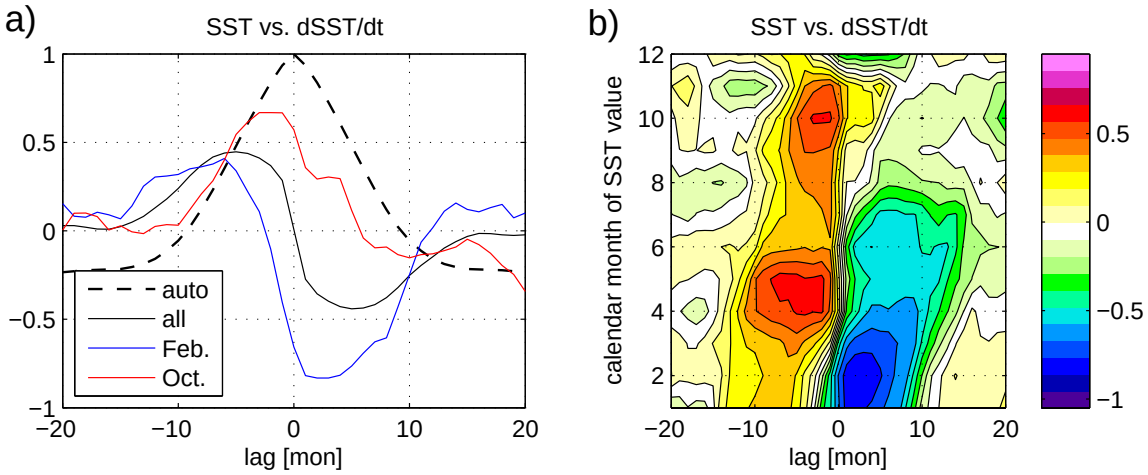

Figure 2: Left: auto-correlation of NINO3 SST (dotted) and cross-correlations of NINO3 SST with the SST tendencies for all calendar month (black solid), February (blue) and October (red). Right: cross-correlations of NINO3 SST with the SST tendencies vs calendar month of SST. Positive lags indicate the SST is leading the SST tendencies and the calendar month is relative to the SST.

Figure 3

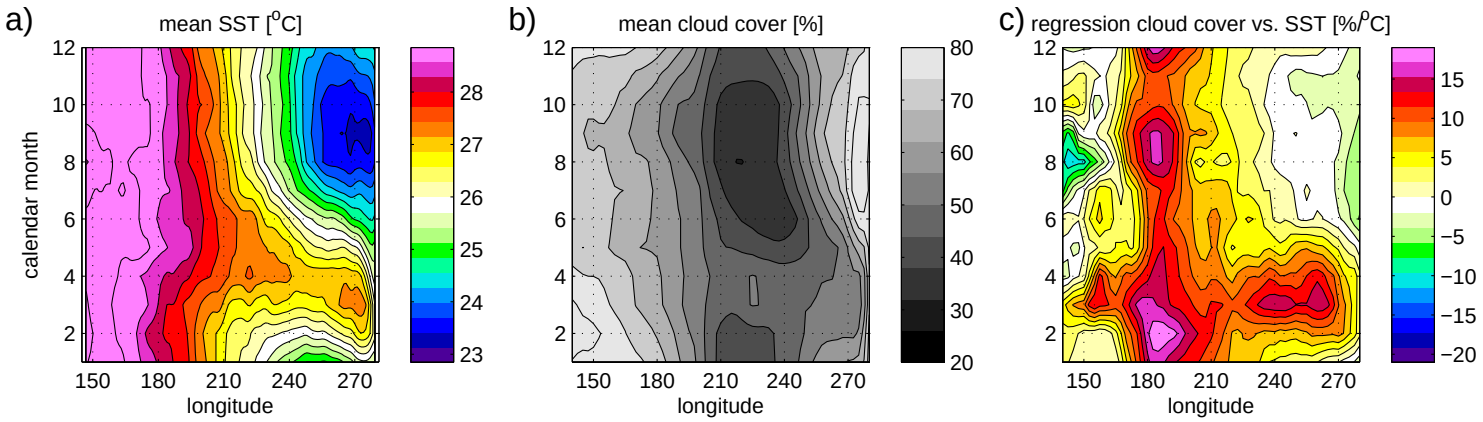

Figure 3: (a) mean SST along the equator. (b) mean cloud cover. (c) regression of cloud cover on SST. Averaging is done from 5^oS to 5^oN.

Figure 4

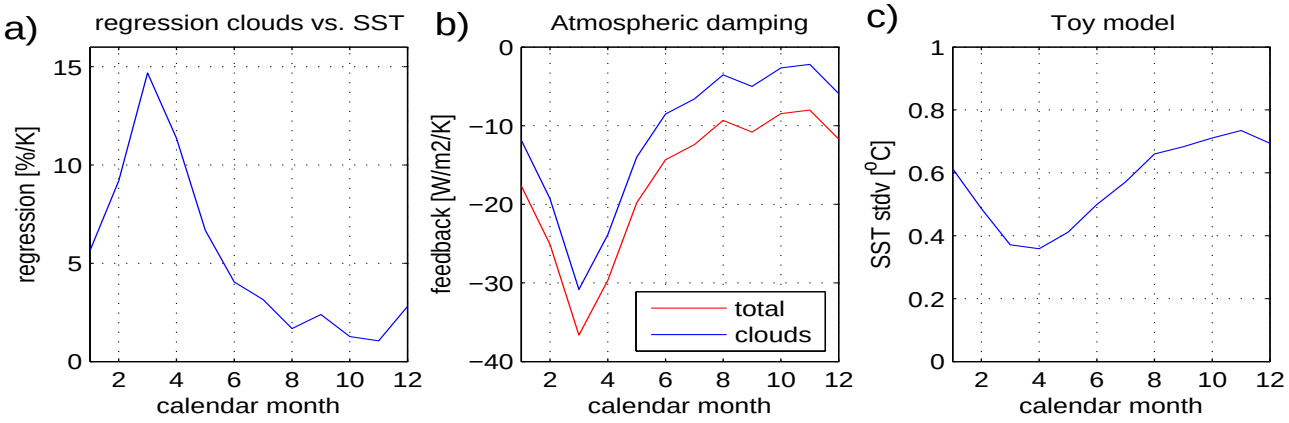

Figure 4: Simple cloud feedback model: (a) linear regression of total cloud cover to SST in the NNINO3 region (mean of the values shown in Fig. 3). (b) Linear atmospheric damping parameter. (c) SST standard deviation in the simple cloud feedback toy model. See text for details.

Figure 5

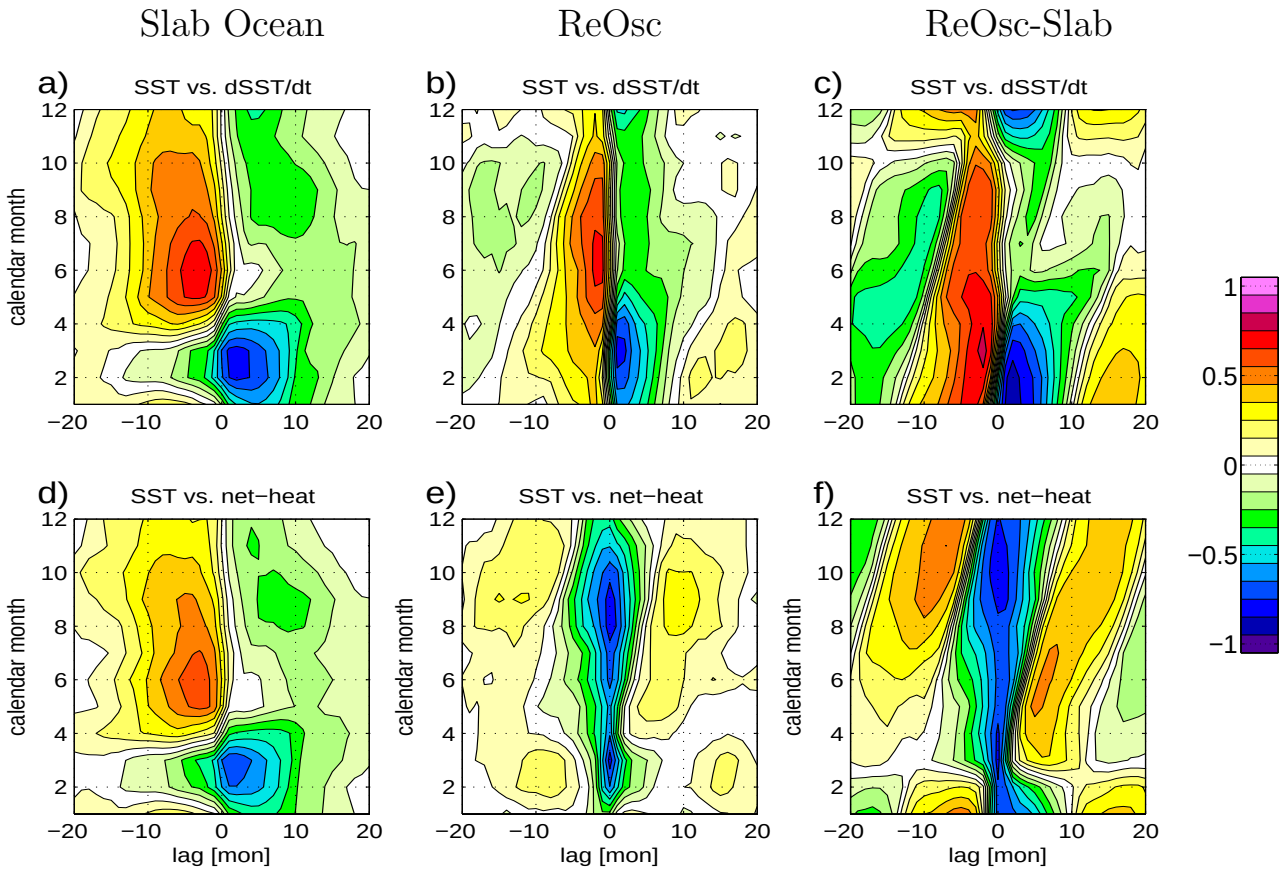

Figure 5: Seasonal cross-correlations: upper row: between SST and SST tendencies. Lower row: between SST and net heat flux. First column for the Slab, second ReOsc and third for the ReOsc-Slab simulation. Positive lags indicate the SST is leading and the calendar month is relative to the SST.

Figure 6

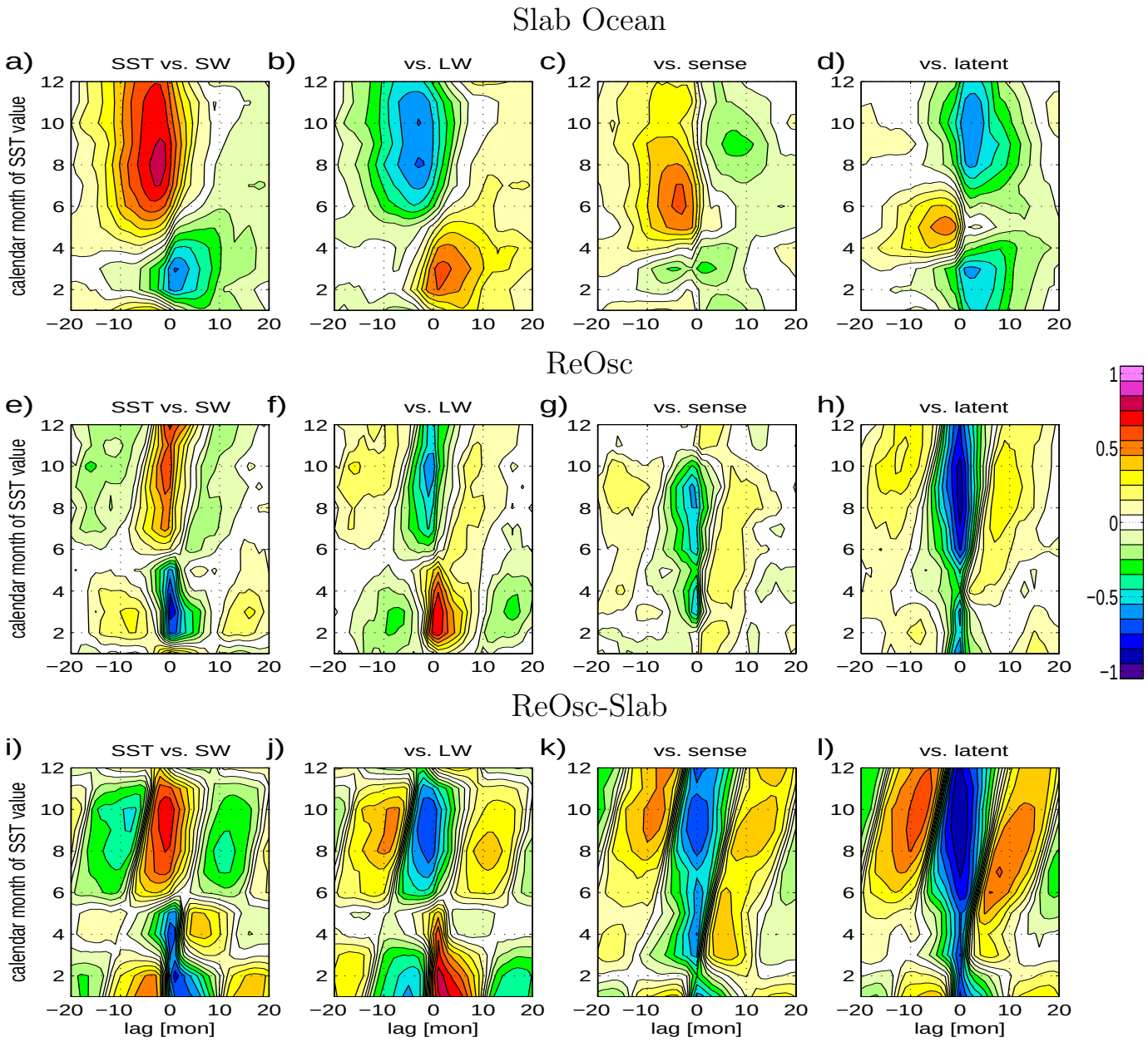

Figure 6: Seasonal cross-correlation between SST and the heat flux components, SW (first column), LW (second column), sensible heat (third column) and latent heat (last column) for the Slab Ocean (first row), ReOsc (second row) and the ReOsc-Slab simulation (last row). Positive lags indicate the SST leading the heat flux evolution.

Figure 7

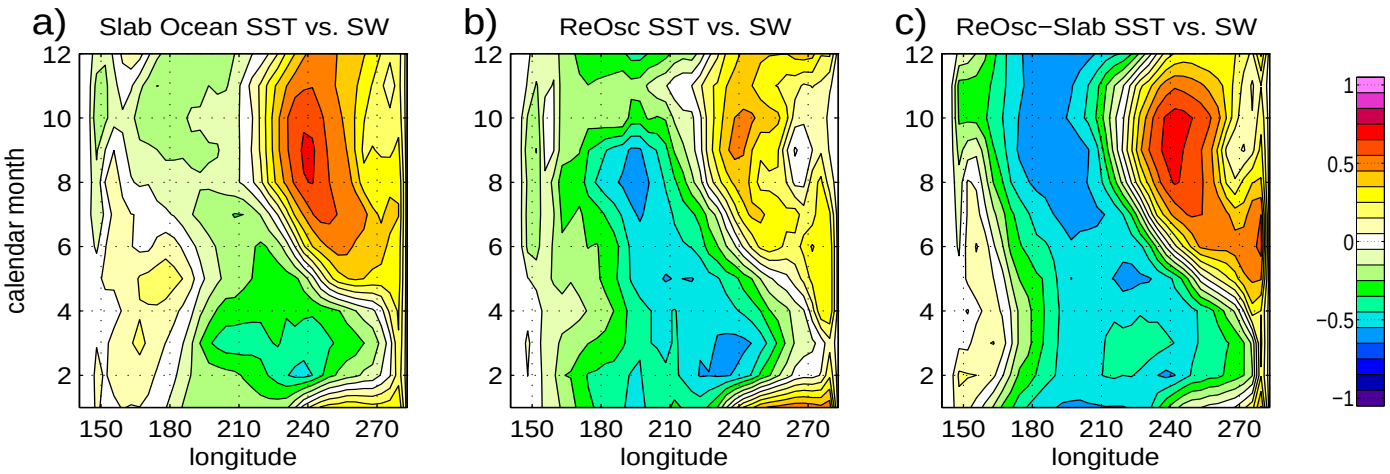

Figure 7: Seasonal cross-correlation between SST and short wave along the equator ($5^oS - 5^oN$) for the Slab Ocean (a), ReOsc (b) and the ReOsc-Slab simulation (c).

Figure 8

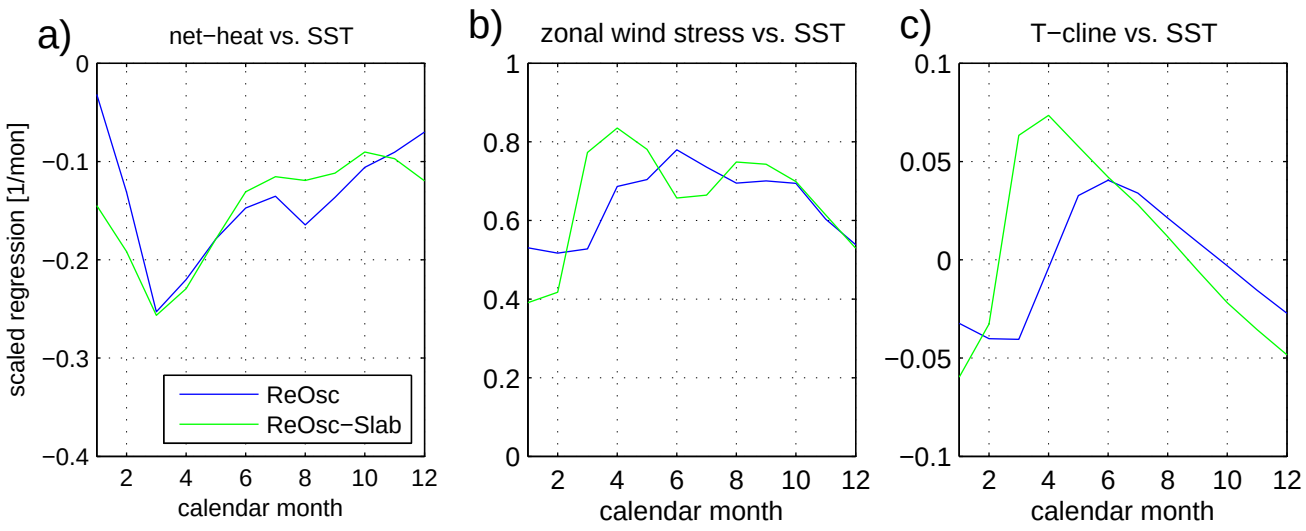

Figure 8: Seasonal regressions in the ReOsc (blue lines) and ReOsc-Slab (green lines) simulations: NINO3 SST vs. net heat (a), zonal wind stress in the central Pacific vs. NINO3 SST (b) and thermocline depth vs. NINO3 SST (c). All regression values are scaled by the corresponding parameters in eq. [4] to have the same scale in terms of monthly SST tendencies per SST.

Figure 9

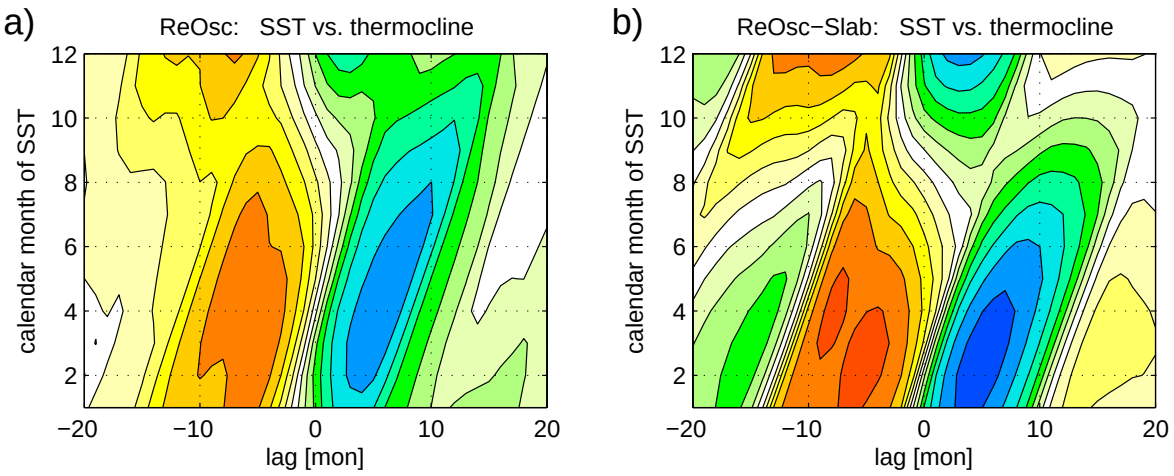

Figure 9: Seasonal cross-correlation between thermocline depth and SST in the ReOsc (a) and ReOsc-Slab simulation (b). Positive lags indicate the SST leading the thermocline depth evolution and the calendar month is relative to the SST.

Figure 10

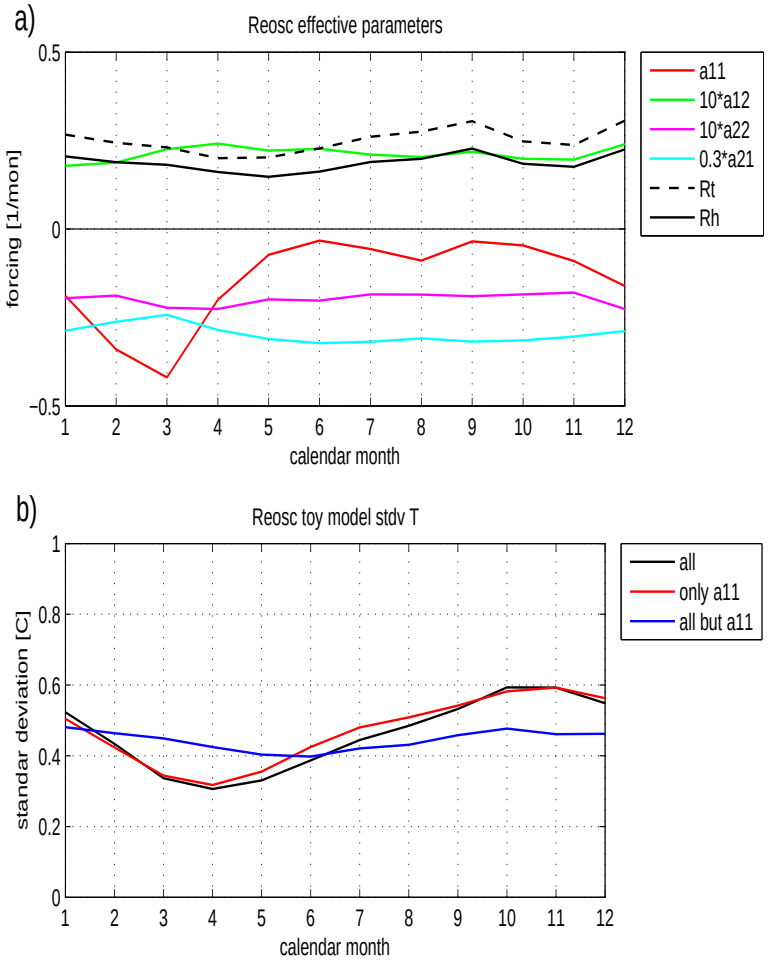

Figure 10: (a) The effective seasonal recharge oscillator parameters (eqs.[1] and [2]) estimate from the ReOsc simulation. (b) Seasonally resolved NINO3 SST standard deviation of a monte carlo integration of the recharge oscillator model (eqs.[1] and [2]) with different combinations of the effective seasonal parameters in (a). See text for details.